Available online at www.sciencedirect.com
ScienceDirect
Trans. Nonferrous Met. Soc. China 30(2020) 1183−1194
Transactions of Nonferrous Metals Society of China
www.tnmsc.cn

Optimization of mechanical properties using D-optimal factorial design of experiment: Electromagnetic stir casting process of A357−SiC nanocomposite

Reza MOHAMMADI BADIZI, Amir PARIZAD, Mohsen ASKARI-PAYKANI, Hamid Reza SHAHVERDI

Department of Materials Engineering, Tarbiat Modares University, P.O. Box 14115-143, Tehran, Iran

Received 9 June 2019; accepted 1 March 2020

Abstract: Electromagnetic stir casting process of A357−SiC nanocomposite was discussed using the D-optimal design of experiment (DODOE) method. As the main objective, nine random experiments obtained by DX-7 software were performed. By this method, A357−SiC nanocomposites with 0.5, 1.0 and 1.5 wt.% SiC were fabricated at three different frequencies (10, 35 and 60 Hz) in the experimental stage. The microstructural evolution was characterized by scanning electron and optical microscopes, and the mechanical properties were investigated using hardness and room-temperature uniaxial tensile tests. The results showed that the homogeneous distribution of SiC nanoparticles leads to the microstructure evolution from dendritic to non-dendritic form and a reduction of size by 73.9%. Additionally, based on DODOE, *F*-values of 44.80 and 179.64 were achieved for yield stress (YS) and ultimate tensile strength (UTS), respectively, implying that the model is significant and the variables (SiC fraction and stirring frequency) were appropriately selected. The optimum values of the SiC fraction and stirring frequency were found to be 1.5 wt.% and 60 Hz, respectively. In this case, YS and UTS for A357−SiC nanocomposites were obtained to be 120 and 188 MPa (57.7% and 57.9 % increase compared with those of the as-cast sample), respectively.

Key words: A357 alloy; electromagnetic stir casting; SiC nanoparticles; mechanical properties; D-optimal design of experiments

1 Introduction

Aluminum metal matrix composites (MMCs) are a major group of structural materials used in aerospace, automobile, and electricity industries due to their light weight, attractive mechanical properties, high corrosion resistance and high thermal conductivity [1,2]. Normally, the addition of micron-sized ceramic particles, such as SiC, Al_2O_3 and TiB_2, improves the yield stress (YS) and ultimate tensile strength (UTS) of aluminum MMCs. However, the ductility deteriorates considerably following the addition of these particles [3]. To deal with the problem, nano-sized ceramic particles were incorporated into the aluminum MMCs to enhance YS and UTS while maintaining the ductility at desirable levels [4]. Methods to fabricate aluminum matrix nanocomposites can be classified into three different groups, i.e., solid state (powder metallurgy, and diffusion bonding), semi-solid state (compocasting), and liquid metallurgy (stir casting, electromagnetic stir casting and in situ processing) [1−5]. The electromagnetic stir casting (ESC) process (liquid metallurgy route) is in preference to other fabrication routes due to its cost-effectiveness, industrialization capability and simplicity [6,7]. Even though the process is generally simple, achieving a homogeneous distribution of the nanoparticles in the matrix is still the main challenge because nanoparticles tend to agglomerate and form large clusters which cannot

Corresponding author: Hamid Reza SHAHVERDI; Tel: +98-2182883307, +98-9125020610; E-mail: shahverdi@modares.ac.ir
DOI: 10.1016/S1003-6326(20)65288-8

be easily wetted by the melt [8]. This feature consequently reduces the mechanical properties and the quality of the composite components [9]. KUMAR et al [10] fabricated A359−Al_2O_3 MMS using ESC. They reported that with increasing the mass fraction of Al_2O_3, the tensile strength of the as-cast composites was greatly improved. DWIVEDI et al [11] reported that the SiC particles distributed in the A357 alloy with the use of an electromagnetic stirrer and showed that the microstructure of alloy became more homogeneous by increasing the intensity of the magnetic field. Also, they indicated that UTS and hardness, increased by 33.1% and 38.2%, respectively, for A357−15.0wt.%SiC composite. MOHAMMADI BADIZI et al [12] investigated the effect of shear rate (electromagnetic stirrer frequency) on the mechanical properties of A357−1.5wt.%SiC nano-particle. They indicated that following an increase in frequency, the hardness and UTS of the A357−1.5wt.%SiC were increased by 30.9% and 57.9%, respectively, compared with the as-cast sample.

The electromagnetic stirrer frequency, stirring time and temperature, and mass fraction of reinforcement (SiC nanoparticles) are the principal parameters affecting the final microstructure of the solidified slurry during the ESC process. It is vital to identify the best combination of electromagnetic parameters to attain the favorable distribution and mechanical properties. The optimization of distribution for the electromagnetic process using this approach is considerably expensive and time-consuming. The most effective combination of the factors may be chosen using the design of experiment (DOE) [13,14]. DOE is a useful method for controlling the distribution and predicting the mechanical properties. Unlike standard classical designs, e.g., fractional factorials, DODOE is typically non-orthogonal, and it is consistently an option regardless of the type of the model chosen by the researchers [15,16]. The optimality criterion used in generating DODOE results in the minimization of the generalized variance of the parameter estimated for a pre-specified model [17]. KHOSRAVI et al [18] optimized the SiC particle distribution during the compocasting of A356−SiC_p composites using DODOE. They found that the SiC particle content of 15 wt.%, stirring temperature of 590 °C, stirring speed of 500 r/min, and stirring time of 30 min were the optimum parameter values, producing the best distribution of the SiC particles in the matrix.

In this study, DODOE was employed to optimize the distribution of SiC nanoparticles and predict mechanical properties in the ESC process of A357−SiC nanocomposite. Among the candidate variables (namely, electromagnetic stirrer frequency, stirring time and temperature, and mass fraction of reinforcement), stirrer frequency and mass fraction of reinforcement were selected as the variables which are likely to have the most influence on the distribution of nanoparticle and mechanical properties of A357−SiC nanocomposite in the ESC process.

2 Experimental

2.1 Materials

A357 alloy with the chemical composition presented in Table 1, was used as the matrix for the fabrication of A357−SiC nanocomposites. In the first level, a blend of SiC nanoparticles (average size of 50 nm) and pure aluminum powder (average size of 50 μm) were pressed into a disk (diameter of 10 mm) under 15 MPa to increase the wettability of SiC nanoparticles with the A357 alloy melt and to improve the distribution of nanoparticles in the melt. In the second level, to produce the A357−SiC nanocomposite, the mixture of A357 and the disks were melted, and electromagnetic stirring was conducted in a graphite crucible in a resistance furnace at 750 °C under three different frequencies (10, 35, and 60 Hz) for 30 min. The furnace was equipped with a vacuum chamber (1.06 Pa). The SiC nanoparticles with the fraction of 0.5, 1, and 1.5 wt.% were added to the A357 matrix. A schematic of the electromagnetic stirrer and detailed information are depicted in Fig. 1. All samples were solidified without electromagnetic stirring via a cylindrical steel mold of A-106 (10 cm × 2 cm). Before microstructure testing, the surfaces of the samples were ground using SiC abrasive papers and then mechanically polished using a 0.3 μm alumina suspension for about 15 min. Eventually, the as-cast samples were etched via a solution containing 2 mL

Table 1 Chemical composition of A357 alloy (wt.%)

Si	Mg	Ti	Fe	Cu	Zn	Mn	Be	Al
7.00	0.60	0.20	0.15	0.05	0.05	0.03	0.05	Bal.

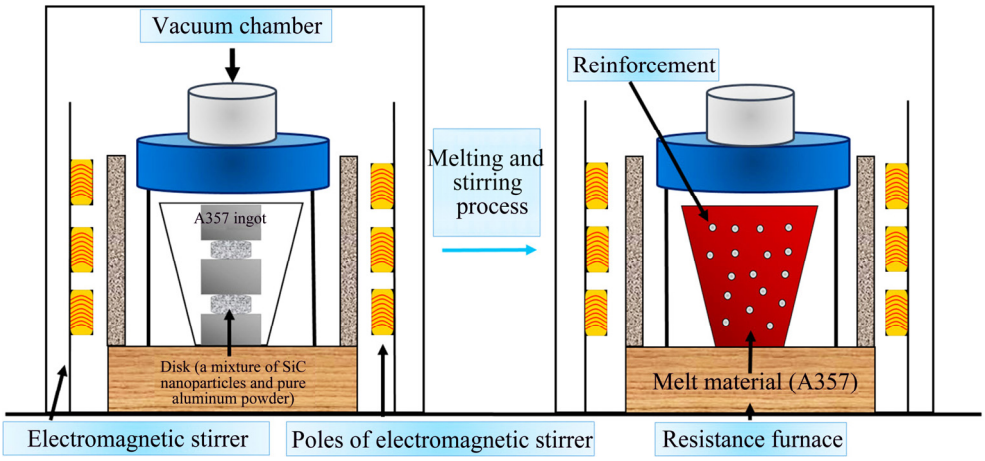

Fig. 1 Schematic of electromagnetic stirrer

of fluoric acid, 3 mL of chloric acid, 5 mL of nitric acid, and 190 mL of distilled water. Optical microscopy (OM) and field emission gun scanning electron microscope (FEGSEM) were utilized to study the microstructural evolution. In addition, A Philips X'Pert PRO X-Ray diffractometer (XRD) using Co K_α (λ=0.179 nm) was used to verify the structure of the samples. The continuous mode, with a holding time of 0.8 s at each 0.02° step size in 2θ=20°−100° was used. The microstructural features of the samples were measured using image analyzer software (Image J software). All the dimensions were evaluated using over ten different images from various areas of the samples, and each dimension was the average value of at least 50 measured data points. The mechanical properties of the samples were characterized using hardness and room-temperature uniaxial tensile tests. The hardness value of the samples was defined using the Brinell scale with a 62.5 kg load for 20 s. The uniaxial tensile tests were carried out in a Ball-Screw/Al-7000-LA universal testing machine with a maximum load capacity of 20 kN at a strain rate of 8.2×10^{-4} s^{-1} based on ASTM-E8. The gauge length and width were 20 and 4 mm, respectively. Three samples for each sample code were evaluated using tensile and hardness tests, and then the mean values were reported.

2.2 Design of experiment

The DOE mainly aims to decrease the number of experiments needed to identify variables influencing the experimental results by applying a statistical design method [19]. The methods of DOE were chosen by considering factors such as the variable interactions, the level of variables, the number of variables, and the number of permissible experiments [19]. Among all the variables of the ESC process, namely, stirring time and temperatures, stirring frequency, and mass fraction of reinforcement, the last two factors have been selected in this study. The DODOE was selected as the experimental design method to recognize the significant factors which are likely to affect the results. The selected factors with their levels and the related experiments are shown in Tables 2 and 3, respectively. According to the DOE, the response for the quadratic polynomials is

$$Y=b_0+\sum b_iX_i+\sum b_{ij}X_iX_j+\sum b_iX_i^2+\acute{\varepsilon} \quad (1)$$

where i and j vary from 1 to the number of variables, b_0 is a coefficient representing the mean of responses from all experiments, b_i is a coefficient representing the effect of variable X_i, b_{ij} is the coefficient of regression that represents the interaction effect of variables X_i and X_j [19], and $\acute{\varepsilon}$ is the error. The interaction effect is the failure of one variable to produce the same effect on the response at different levels of another variable [19]. Design-Expert 7 (Stat-Ease, Inc., Trial version) software was used to perform multiple regression analyses, analysis of variance (ANOVA), and ridge analysis of the maximum of information during the response surface method.

Table 2 Selected factors and their levels

Selected factor	Symbol for factor	Level		
		−1	0	1
SiC content/wt.%	A	0.5	1.0	1.5
Frequency/Hz	B	10	35	60

Table 3 D-optimal DOE: Experimental sequences and responses

Sample No.	SiC content/ wt.%	Stirring frequency/Hz	Yield stress/MPa		UTS/MPa	
			Calculated by experiment	Calculated by Eq. (2)	Calculated by experiment	Calculated by Eq. (3)
1	0.5	10	89	88.3	135	134.7
2	1.0	10	94	94.3	140	141
3	1.5	10	71	69.9	101	99.7
4	0.5	35	98	94.8	144	143.2
5	1.0	35	110	110.3	170	171
6	1.5	35	90	94.8	139.2	143.2
7	0.5	60	102	101.3	152	157
8	1.0	60	103	102.3	158	156
9	1.5	60	120	119.8	188	186.7

3 Results and discussion

3.1 Analysis of design of experiment

The present study demonstrates the effect of electromagnetic stirring frequency and mass fraction of SiC nanoparticles on the mechanical properties (YS and UTS) of A357−SiC nanocomposite during the ESC process via DODOE. The results of YS and UTS testing are presented in Tables 4 and 5, respectively, with a confidence interval (CI) of 95% for the model. In statistics, CI is a kind of interval estimate for a population parameter and is used to illustrate the reliability of an estimate. The confidence level of CI would show the probability that the confidence range captures this true population parameter given the distribution of samples [16,17]. Considering normal and half normal plots, the principal effects and two-factor interactions all with CI of 95% were chosen as the main factors for modeling. The effect of a factor is determined as the change in response as the result of a variation in the level of the factor. This is frequently called the main effect because it refers to the primary factors of interest in the experiment [19]. ANOVA results for YS indicated the significance of the model with adequate precision of 22.621. Adequate precision compares the span of the forecasted values at the design points to the average prediction error and measures the signal to noise ratio (a ratio greater than 4 is considered acceptable) [16]. Here, the value of the ratio is greater than 4, representing the adequacy of the model for predicting the results within the design space without the need for further experiments. The fitting of the equations was measured by the "adjusted *R*-squared" coefficient or, in a better method, by "predicted *R*-squared" coefficient. The "adjusted *R*-squared" values display variability in the observed response values, which can be described by the experimental factors and their interactions. The "predicted *R*-squared" and "adjusted *R*-squared" values are closer to 1, showing a better fit [20].

For YS, the "predicted *R*-squared" value of 0.9782 is in reasonable agreement with the "adjusted *R*-squared" value of 0.9563. The model *F*-value of 44.80 implies that the model is significant, and there is only a 0.14% chance that a large "model *F*-value" could occur due to noise. Values of "Prob > *F*" less than 0.0500 demonstrate that model terms are significant. In this case, *B*, *AB*, A^2, and A^2B are significant model terms. This model (Eq. (2)) should be used to navigate the design space.

$$YS=102.33+8B+9.23AB-7.48A^2+7.72A^2B \quad (2)$$

The relationships between the actual and predicted values are shown in Table 3, which confirm the navigation power of the model. Sum of squares (SS) of each factor quantifies its matter in the process, and as the value of the SS increases, the significance of the corresponding factor in the undergoing process also rises. As shown in Table 4, the effect of *AB* (SiC fraction × stirrer frequency) is the strongest, followed by *B*, A^2, and A^2B, respectively. Significant factors in the fitted model (Eq. (2)) were selected as the axes for the 3D plots (Fig. 2). In a contour plot (base plots in the 3D plot), curves of the equal response values are drawn

Table 4 Analysis of variance with CI of 95% for model and factors (yield stress)

Source	Sum of squares	DF	Mean square	*F*-value	*P* > *F*	Significance
Model	1569.51	4	392.38	44.80	0.0014	Significant
B	128.00	1	128.00	14.61	0.0187	
AB	340.40	1	340.40	38.86	0.0034	
A^2	112.00	1	112.00	12.79	0.0233	
A^2B	79.57	1	79.57	9.08	0.0394	
Residual	35.04	4	8.76			
Cor total	1604.54	8				

Table 5 Analysis of variance with CI of 95% for model and factors (UTS)

Source	Sum of squares	DF	Mean square	*F*-value	*P* > *F*	Significance
Model	4706.68	4	1176.67	179.64	0.0001	Significant
B	450.00	1	450.00	68.70	0.0012	
AB	1225.00	1	1225.00	187.02	0.0002	
A^2	327.68	1	327.68	50.03	0.0021	
A^2B	161.33	1	161.33	24.63	0.0077	
Residual	26.20	4	6.55			
Cor total	4732.88	8				

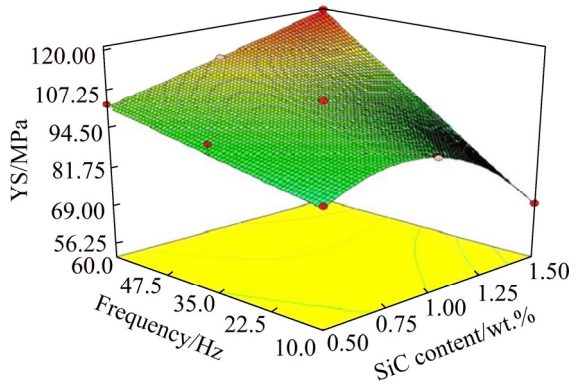

Fig. 2 3D plot of yield stress as function of frequency and SiC content

on a plane, whose coordinates represent the levels of the independent factors. Each contour represents a particular value for the height of the surface above the plane determined for a combination of the levels of the factors. Consequently, different surface heights enable the focus of attention on the levels of the factors at which changes in the surface height occur [21,22]. Figure 2 shows that YS slightly increases following a rise in frequency, and it has a parabolic relationship with SiC content. Put it another way, high YS could be earned by high frequency and SiC content close to level 1 of other factors (see Table 2).

Also, ANOVA results of the UTS confirm the significance of the model with adequate precision of 45.607. The "predicted *R*-squared" value of 0.9945 is in reasonable agreement with the "adjusted *R*-squared" value of 09889. The model *F*-value of 179.64 implies that the model is significant, and there is only a 0.01% chance that a large "model *F*-value" could occur due to noise. Values of "Prob > *F*" less than 0.0500 demonstrate that model terms are significant. In this case, *B*, *AB*, A^2, and A^2B are significant model terms. As shown in Table 5, *AB* (SiC content × stirrer frequency) has the strongest effect, followed by *B*, A^2, and A^2B, respectively. This model (Eq. (3)) should be used to navigate the design space.

$$UTS=156+15B+17.5AB-12.8A^2+11A^2B \quad (3)$$

Figure 3 shows that UTS is improved by increasing frequency, and it has a parabolic relationship with SiC content. This means that high UTS could be obtained by high frequency and SiC content (Table 2).

Generally, the confirmation experiments were carried out under three different conditions. The results are shown in Table 6. If the average of

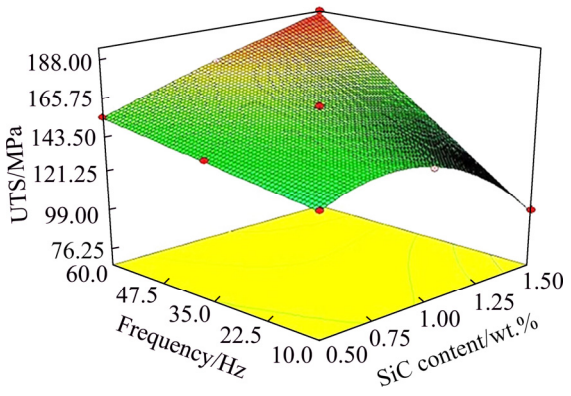

Fig. 3 3D plot of UTS as function of frequency and SiC content

confirmation results is within the limits of the CI, then the significant factors and the levels for obtaining the desired results are proved to be correctly chosen [15,16]. As observed in Table 6, the experimental responses are in the 95% CI range; hence, this model can be used to navigate within the design space. Optimum conditions of the experiment are as follows: A=1.5 wt.% and B= 60 Hz. Under this condition, the YS and UTS were obtained to be 120 and 188 MPa, respectively. The increase in YS and UTS can be attributed to the homogeneous distribution of SiC nanoparticles and microstructure evolution.

3.2 Metallurgical characterization

3.2.1 Effect of stirring frequency in ESC process

The A357−1.5 wt.%SiC was stirred at three different frequencies (10, 35 and 60 Hz). OM micrographs of the as-cast A357 alloy and A357−1.5 wt.%SiC nanocomposite fabricated at the stirring frequency of 60 Hz by electromagnetic stirrer are shown in Fig. 4. It is obvious that the main microstructural feature of the as-cast A357 alloy is a dendritic structure consisting of primary α(Al) dendrites and Al−Si eutectic phases at the interdendritic zones (Fig. 4(a)). It is worth mentioning that due to the lower thermal conductivity and heat diffusivity of SiC ceramic nanoparticles compared with the matrix alloy, the nanoparticles are cooled down more slowly during solidification than the melt. The higher temperature at the vicinity of the particles leads to the nucleation of α dendrites far from the particles, i.e., in the case of lower melt temperature. Then, the residual liquid becomes enriched with Si and other solutes, and the solidification is completed by nucleation of Al−Si eutectic phase on the SiC nanoparticles surface which can act as a desirable site for heterogeneous nucleation [3,5]. It is clear that by reinforcing the alloy with SiC nanoparticles, micro-structure changes from dendritic shape to equiaxed form (Fig. 4(b)). Furthermore, the addition of SiC nanoparticles to the melt refines the microstructure. These microstructural characteristics are directly related to the stirring process of the melt, in which α(Al) dendrites are broken by the melt shear flow created by electromagnetic forces [5]. Microstructure refinement can also be ascribed to the role of SiC nanoparticles. It has been reported that these nanoparticles provide some heterogeneous nucleation sites which enhance the nucleation of new grains during solidification. Moreover, the SiC nanoparticles located at the grain boundaries can preclude the migration of grain boundaries and consequently limit the grain coarsening [23,24]. Figure 5 shows the XRD pattern of the as-cast A357 alloy and that of A357−1.5 wt.%SiC at the stirring frequency of 60 Hz. As evident in Fig. 5(b), the existence of SiC peaks verifies the presence of SiC nanoparticles in the aluminum matrix. Moreover, Al and Si peaks detected in both patterns indicate the presence of α(Al) and Al−Si eutectic phases, respectively.

Figure 6 depicts the distribution of SiC nanoparticles and microstructures of A357−SiC nanocomposites fabricated at two different stirring frequencies, i.e., 35 and 60 Hz. It is clear that the best distribution of SiC nanoparticles is obtained at the stirring frequency of 60 Hz with 1.5 wt.% of

Table 6 Results of confirmation tests

Confirmation test No.	A/wt.%	B/Hz	Yield stress/MPa		UTS/MPa	
			Pred.	Exp.	Pred.	Exp.
1	0.5	60	101.3	102	157	152
2	1.0	35	110.1	110	171	170
3	1.0	60	102.3	103	156	158

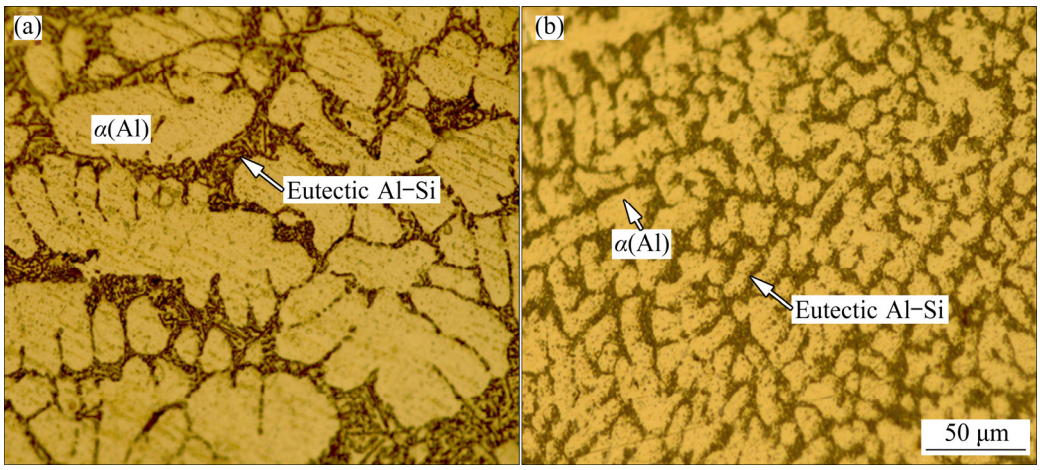

Fig. 4 Optical micrographs of unreinforced A357 alloy (a) and A357−1.5wt.%SiC nanocomposite fabricated at stirring frequency of 60 Hz (b)

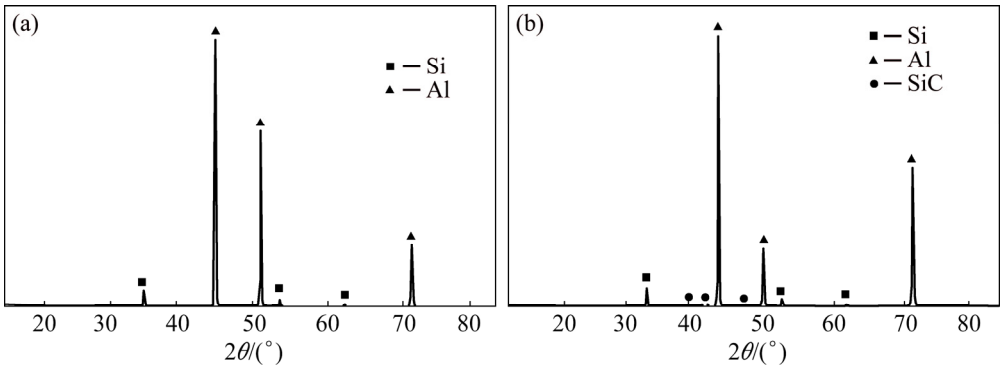

Fig. 5 XRD patterns of unreinforced A357 alloy (a) and A357−1.5wt.%SiC nanocomposite fabricated at stirring frequency of 60 Hz (b)

SiC nanoparticles (Fig. 6(d)). It is well-known that in the composites fabrication process, nanoparticles are more susceptible to clustering because of the higher surface area and surface energy. In this work, these features are more dominant in the case of nanocomposite samples fabricated at the stirring frequency of 10 Hz, i.e., in case that the shear force produced within the melt by the electromagnetic force fails to be enough for nanoparticles distribution [12]. The tensile properties of the as-cast A357 alloy and nanocomposite samples are exhibited in Fig. 7. It can be easily understood that the addition of SiC nanoparticles to the A357 alloy matrix improves the UTS without sacrificing the ductility. Another aspect easily observed in the figure is the influence of stirring frequency on the tensile properties of the nanocomposite samples. Heterogeneous distribution of SiC nanoparticles in Sample 3 and increased porosity caused by the lack of enough electromagnetic stirrer frequency power led to a decrease in YS, UTS, and ε_f to (71±5.1) MPa, (101±4.5) MPa, and (4.1±1.0)%, respectively. The homogeneous distribution of SiC nanoparticles in Samples 6 and 9 resulted in the improved tensile properties (Fig. 6). Following a rise in frequency from 35 to 60 Hz, YS, UTS, and ε_f for Samples 6 and 9 also increased from (90±2.2) MPa, (139.2±3.0) MPa, and (6.0±1.8)% to (120±2.5) MPa, (188±3.2) MPa, and (18±4.7)%, respectively. The improvement in tensile properties following an increase in stirring frequency can be attributed to the microstructure refinement and uniform distribution of nanoparticles within the matrix, which reduces the spacing among particles; this feature also inhibits the dislocation motion and consequently enhances the strength [25]. As mentioned earlier, nanocomposite samples such as Sample 3 include agglomerated particles which are the most suitable sites for damage accumulation and crack nucleation [26].

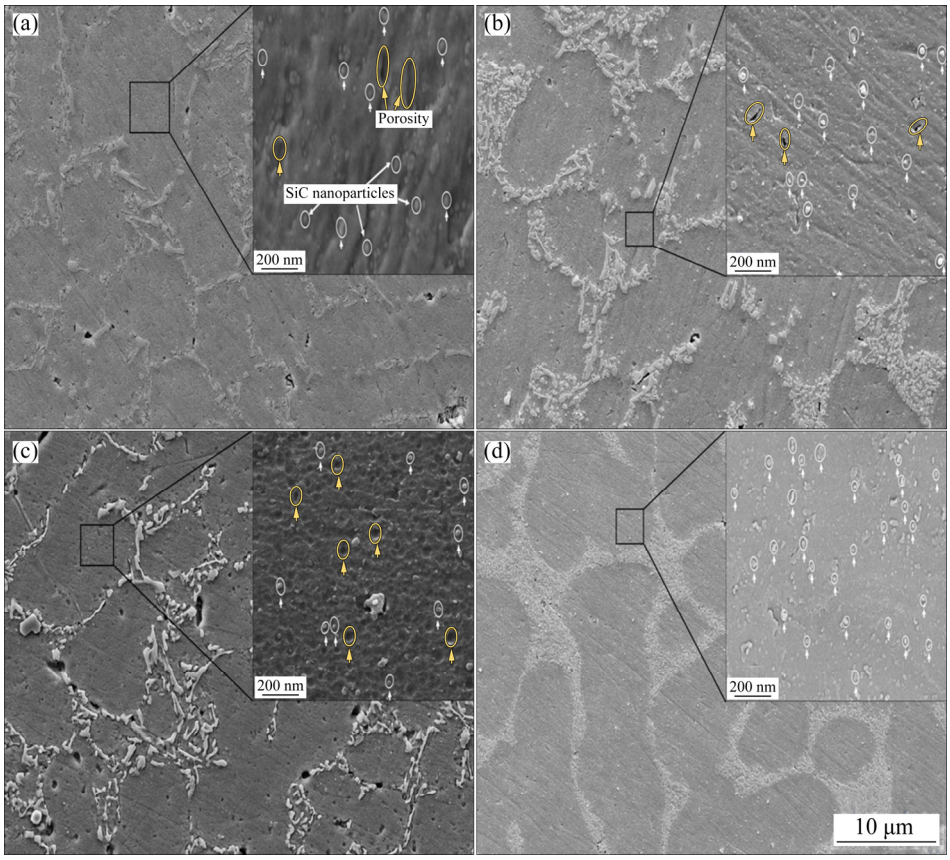

Fig. 6 FESEM micrographs of A357 matrix alloy reinforced with various contents of SiC nanoparticles under various stirring frequencies corresponding to Samples 7 (a), 5 (b), 8 (c), and 9 (d) in Table 3, respectively

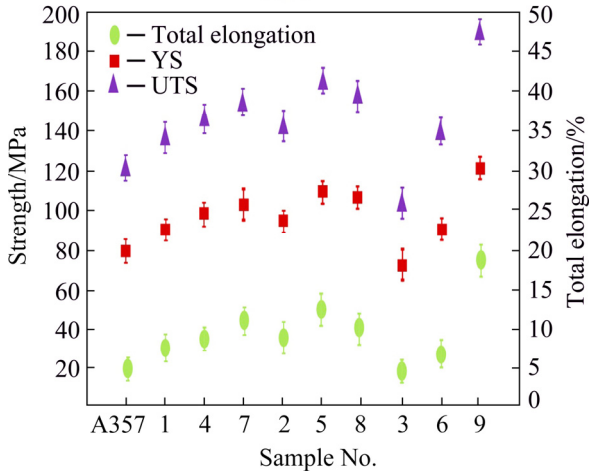

Fig. 7 Strength and total elongation of as-cast and nanocomposite samples

3.2.2 Effect of SiC content in ESC process

At the stirring frequency of 60 Hz the nanocomposite samples were fabricated with 0.5, 1.0 and 1.5 wt.% of SiC nanoparticle. In samples with 0.5 and 1.0 wt.% of nanoparticles, porosity formation is more prevalent (Figs. 6(a) and (c)). Generally, some of the main principles which can contribute to porosity formation are as follows: (1) particle size reduction, which increases the surface area in contact with air; (2) gas entrapment during stirring; (3) the pouring distance from the crucible to the mold, and (4) solidification shrinkage [3]. In this study, the formation of porosities can be mainly ascribed to the gas entrapment because of stirring at a higher frequency and it is not favorable for low content of SiC nanoparticles (like 0.5 wt.%). In addition, with increase of SiC nanoparticles (0.5 to 1.5 wt.%) and homogeneous distribution at appropriate stirring frequency, the microstructure of A357−SiC nanocomposite refines and reduces the average grain size. The most pronounced effect can be observed in A357−1.5wt.%SiC at the stirring frequency of 60 Hz, in the case where a grain size reduction of about 73.9% is evident compared with the as-cast A357 alloy (grain size reduces from (59.5±1.8) μm to (15.5±3.6) μm). The variation in nanocomposite grain size and reduction of grain size compared with the as-cast A357 alloy is shown in Table 7. As mentioned earlier, stirring the melt

provides the uniform distribution of SiC nanoparticles. These small particles can favorably act as heterogeneous nucleation sites during the solidification process. This occurrence not only reduces the grain size but also changes the structure from dendritic to equiaxed form [27,28]. Evaluation of the structure from dendritic to equiaxed form leads to the improvement of mechanical properties. According to Fig. 7 it can be seen that YS, UTS, and elongation (ε_f) of the nanocomposite samples with 0.5 and 1.0 wt.% of SiC at the stirring frequencies of 10 and 35 Hz slightly increase in comparison with the as-received A357 alloy.

Table 7 Grain size evolution

Sample No.	SiC content/ wt.%	Frequency/ Hz	Grain size/μm	Reduction/ %
A357	0	0	59.5±1.8	0
1	0.5	10	50.3±2.5	15.4
4	0.5	35	39.5±1.8	33.6
7	0.5	60	43.3±3.3	27.2
2	1.0	10	33.2±3.1	44.2
5	1.0	35	22.0±2.9	63.0
8	1.0	60	28.6±3.4	51.9
3	1.5	10	34.9±3.7	41.3
6	1.5	35	29.5±4.8	50.4
9	1.5	60	15.5±3.6	73.9

In order to study the effect of mass fraction and the distribution homogeneity of SiC nanoparticles, the Brinell hardness measurements were conducted along the longitudinal direction of casting (from top to bottom) on the cross-section of the fabricated nanocomposites. Figure 8 shows the schematic of the selected positions, and Fig. 9 displays the Brinell hardness. As clearly observed, there is no substantial variation in the hardness across the cross-section for nanocomposites samples. Therefore, it can be concluded that SiC nanoparticles have been homogeneously distributed throughout the microstructure during the electromagnetic stir casting process. Referring to the above discussion, the hardness of nanocomposites slightly increases following a rise in the SiC content. Typically, the higher hardness of the nanocomposites is related to both the grain refinement (Hall−Petch theory) and the role of SiC nanoparticles acting as barriers to the dislocation motion (Orowan mechanism) [29].

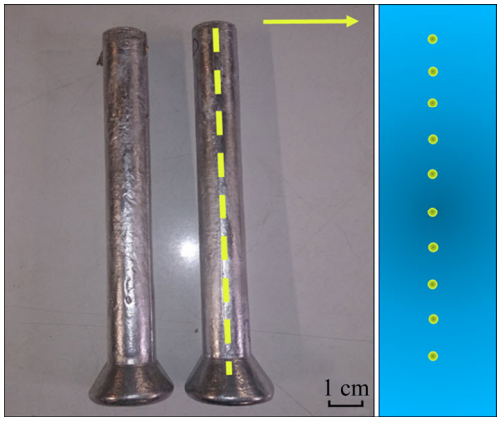

Fig. 8 Schematic illustration of selected positions on cross-section of nanocomposite samples

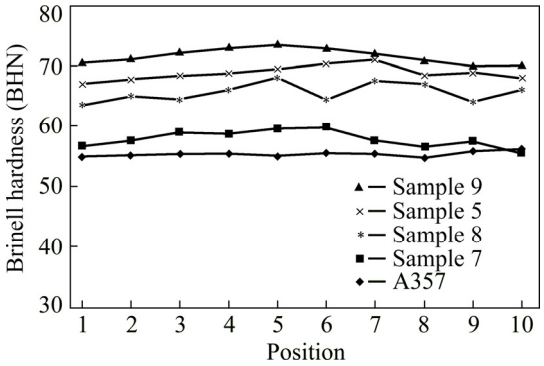

Fig. 9 Brinell hardness values of nanocomposite samples

In this research, with increasing SiC content from 0 to 1.5 wt.% at frequency of 60 Hz, the hardness also increases from 55.3 to 72.4 (30.9% increase compared with the as-cast sample). Also, more fluctuation in hardness value in some samples (Sample 8) (Fig. 9) can be due to an increase in porosity. An increase in the hardness at various stirring frequencies and mass fraction of SiC nanoparticles due to the homogenous distribution of SiC nanoparticles and decrease can be attributed to the clustering and the presence of more porosity [30,31].

As discussed in Sections 3.1 and 3.2, SiC content (A) and stirring frequency (B) directly affect the simultaneous increase in YS and UTS. However, the best mechanical properties of A357−SiC nanocomposite due to homogenous distribution (Fig. 6(d)) were achieved in maximum A and B (1.5 wt.% SiC and 60 Hz frequency). It should be notified that the level of stirring frequency is dependent on the SiC content. The optimal mechanical properties (YS and UTS) at 35 Hz were achieved with 1.0 wt.% SiC, leading to

homogenous distribution of SiC nanoparticles (Fig. 6(b)).

3.2.3 Contributions of different strengthening mechanisms

As reported by ZHONG et al [32], the Hall−Petch mechanism, Orowan mechanism, mismatch stress, and load-bearing effect are four different mechanisms which contribute to the increased tensile strength of nanocomposites. The Hall−Petch mechanism demonstrates the contribution of grain size; according to the Hall−Petch equation [33,34], the composite strength increases with decreasing the matrix grain size.

$$\Delta\sigma_{\text{Hall–Petch}}=k/\sqrt{D} \tag{4}$$

where k and D stand for the Hall−Petch coefficient and the grain diameter, respectively.

The distribution of nanoparticles in the matrix leads to the interaction between dislocations and nanoparticles, which subsequently increases the strength (Orowan mechanism). The variation of strength based on the Orowan mechanism can be calculated for SiC nanoparticles as follows [35]:

$$\Delta\sigma_{\text{Orowan}}=\frac{0.13G_{\text{m}}b}{\lambda}\ln\frac{d_{\text{p}}}{2b} \tag{5}$$

where G_{m} is the shear modulus of the matrix, b is the Burgers vector, λ is the inter-particle spacing, and d_{p} is the average diameter of nanoparticles.

Mismatch stress, as the third strengthening mechanism, stems from the difference between the coefficient of thermal expansion (CTE) of reinforcement and that of the matrix. During the solidification process, the residual thermal stress caused by CTE mismatch increases the dislocation density around the reinforcement nanoparticles. This plastic deformation improves the strength of nanocomposite. The effect of mismatch stress due to the difference between the CTE values of nanoparticles and matrix is given by the following equation [32]:

$$\Delta\sigma_{\text{CTE}}=\sqrt{3}\beta G_{\text{m}}b\sqrt{\frac{12V_{\text{p}}\Delta T\Delta\alpha}{(1-V_{\text{p}})d_{\text{p}}b}} \tag{6}$$

where the strengthening coefficient of β equals 1.25, $\Delta\alpha$ is the difference between CTE values of the aluminum matrix and SiC nanoparticles, ΔT is the difference between the processing and the test temperatures, and V_{p} is the volume fraction of the particles.

The load transfer from the metal matrix to the ceramic reinforcements is the last strengthening mechanism. However, the effective load transfer mainly relies on interfacial bonding between the matrix and the reinforcement. Load transfer can be estimated as follows [32]:

$$\Delta\sigma_{\text{Load}}=0.5V_{\text{p}}\sigma_{\text{ym}} \tag{7}$$

where σ_{ym} is the yield strength of matrix. The contribution of each of the above mechanisms to the yield stress improvement of the nanocomposites can be estimated by the following equation [23]:

$$\Delta\sigma=[(\Delta\sigma_{\text{Hall–Petch}})^2+(\Delta\sigma_{\text{Orowan}})^2+(\Delta\sigma_{\text{CTE}})^2+(\Delta\sigma_{\text{Load}})^2]^{1/2} \tag{8}$$

In addition to the mechanical properties prediction by DODOE, the contribution of different strengthening mechanisms to the YS improvement of the A357−1.5wt.%SiC nanocomposite fabricated at 60 Hz was calculated using Eqs. (4) to (8), according to the data presented in Table 8. The respective results are listed in Table 9, where the improvement of final strength equals to 45.18 MPa. This value is close to the experimental value of about 41 MPa obtained from the stress−strain curves.

Table 8 Constant parameters for calculating contribution of different terms to yield stress of Sample 9 [28]

d_{p}/ nm	G_{m}/ MPa	b/ nm	σ_{ym}/ MPa	$\Delta\alpha$/ K^{-1}	ΔT/ K	V_{p}	λ/ nm
50	26500	0.283	79	21×10^{-6}	725	0.012	300

Table 9 Calculated strengtheing proportion of different mechanisms at YS

$\Delta\sigma_{\text{Hall–Petch}}$/ MPa	$\Delta\sigma_{\text{Orowan}}$/ MPa	$\Delta\sigma_{\text{CTE}}$/ MPa	$\Delta\sigma_{\text{Load}}$/ MPa	$\Delta\sigma_{\text{Total}}$/ MPa
10.45	14.55	41.48	0.474	45.18

4 Conclusions

(1) According to the results of DODOE, F-values of 44.80 and 179.64 for YS and UTS, respectively, imply that the model is significant and the chosen variables (SiC fraction and stirring frequency) were appropriately selected.

(2) SiC fraction and stirring frequency are the most effective factors in the ESC process and have a direct effect on the simultaneous increase in YS and UTS. In other words, improvement of the mechanical properties of nanocomposite by increasing the stirring frequency in the ESC process

is dependent on the SiC fraction.

(3) The optimum values of the stirring frequency and SiC fraction were measured to be 60 Hz and 1.5 wt.%, respectively.

(4) The homogeneous distribution of SiC nanoparticles in optimum condition led to microstructure evolution from dendritic to a non-dendritic form and reduction of size to 73.9%.

(5) Hardness, YS, and UTS of the A357−1.5 wt.% nanocomposite (the best nanocomposite sample) stirred at 60 Hz frequency were increased by 30.9%, 57.7%, and 57.9%, respectively, compared with the as-cast samples.

References

[1] OZTURK I, AGAOGLU G H, ERZI E, DISPINAR D, ORHAN G. Effects of strontium addition on the microstructure and corrosion behavior of A356 aluminum alloy [J]. Journal of Alloys and Compounds, 2018, 763: 384−391.

[2] KRISHNAN P K, CHRISTY J V, ARUNACHALAM R, MOURAD A H I, MURALIRAJA R, AL-MAHRABI M, MURALI V, CHANDRA M M. Production of aluminum alloy-based metal matrix composites using scrap aluminum alloy and waste materials: Influence on microstructure and mechanical properties [J]. Journal of Alloys and Compounds, 2019, 784: 1047−1061.

[3] SAJJAD S A, EZATPOUR H R, BEYGI H. Microstructure and mechanical properties of Al−Al_2O_3 micro and nanocomposites fabricated by stir casting [J]. Materials Science and Engineering A, 2011, 528: 8765−8771.

[4] PADHI P, KUMAR K. N, GHOSH S, VISHWANATHA H M, PAWIGRAHI S C, GHOSH S. Modeling and experimental validation of deagglomeration of ultrafine nanoparticles in liquid Al during noncontact ultrasonic casting [J]. Materials and Manufacturing Processes, 2016, 31(12): 1589−1596.

[5] SELVAM J D R, DINAHARAN I, PHILIP S V, MASHININI P M. Microstructure and mechanical characterization of in situ synthesized AA6061/(TiB_2+Al_2O_3) hybrid aluminum matrix composites [J]. Journal of Alloys and Compounds, 2018, 740: 529−535.

[6] LU De-hong, JIANG Ye-hua, GUAN Gui-sheng, ZHOU Rong-feng, LI Zhen-hua, ZHOU Rong. Refinement of primary Si in hypereutectic Al−Si alloy by electromagnetic stirring [J]. Journal of Materials Processing Technology, 2007, 189: 13−18.

[7] MAPELLI C, GRUTTADAURIA A, PERONI M. Application of electromagnetic stirring for the homogenization of aluminum billet cast in a semi-continuous machine [J]. Journal of Materials Processing Technology, 2010, 210: 306−314.

[8] YAN Zhi-ming, CHEN Mei-ling, YANG Jun, YANG Li, GAO Hong. Grain refinement of CuNi10Fe1Mn alloy by SiC nanoparticles and electromagnetic stirring, Mater [J]. Materials and Manufacturing Processes, 2013, 28(8): 957−961.

[9] SHAYAN M, NIROUMAND B. Synthesis of A356−MWCNT nanocomposites through a novel two stage casting process [J]. Materials Science and Engineering A, 2013, 582: 262−269.

[10] KUMAR A, LAL S, KUMAR S. Fabrication and characterization of A359−Al_2O_3 metal matrix composite using electromagnetic stir casting method [J]. Journal of Materials Research and Technology, 2013, 2(3): 250−254.

[11] DWIVEDI P S, SHARMA S, MISHRA K R. Microstructure and mechanical properties of A356-SiC composites fabricated by electromagnetic stir casting [J]. Procedia Materials Science, 2014, 6: 1524−1532.

[12] MOHAMMADI B R, ASKARI-PAYKANI M, PARIZAD A, SHAHVERDI H R. Effects of electromagnetic frequency and SiC nanoparticles on the microstructure refinement and mechanical properties of Al A357−1.5 wt.% SiC nanocomposite [J]. International Journal of Metalcasting, 2018, 12(3): 565−573.

[13] ASKARI-PAYKANI M, SHAYAN M, SHAMANIAN M. Weldability of ferritic ductile cast iron using full factorial design of experiment [J]. Journal of Iron and Steel Research, International, 2014, 1(2): 252−263.

[14] KHAMNEH M E, ASKARI-PAYKANI M, SHAHVERDI H R, HADAVI S M M, EMAMI M. Optimization of spring-back in creep age forming process of 7075 Al-alclad alloy using D-optimal design of experiment Method [J]. Measurement, 2016, 88: 278−286.

[15] ANDERSON M J, WHITCOMB P J. DOE simplified: Practical tools for effective experimentation [M]. Portland: Productivity Inc, 2000.

[16] Software helps Design-Expert Software, Version 7.1, User's guide, Technical Manual, Stat-Ease Inc, Minneapolis, MN, 2007.

[17] NIST/SEMATECH e-Handbook of Statistical Methods. http://www.itl.nist.gov/div898/handbook/, March 2008.

[18] KHOSRAVI H, ESLAMI-FARSANI R, ASKARI-PAYKANI M. Optimization of SiC particle distribution during compocasting of A356−SiC_p composites using D-optimal experiment design [J]. Journal of Particle Science and Technology, 2017, 3: 145−154.

[19] GOTTIPATI R, MISHRA S. Process optimization of adsorption of Cr(VI) on activated carbons prepared from plant precursors by a two-level full factorial design [J]. Chemical Engineering Journal, 2010, 160: 99−107.

[20] COSTA S, BARROSO M, CASTANERA A, DIAS M. Design of experiments, a powerful tool for method development in forensic toxicology: Application to the optimization of urinary morphine 3-glucuronide acid hydrolysis [J]. Analytical and Bioanalytical Chemistry, 2010, 396: 2533−2542.

[21] KHOSRAVI H, ESLAMI-FARSANI R, ASKARI-PAYKANI M. Modeling and optimization of cooling slope process parameters for semi-solid casting of A356 Al alloy [J]. Transactions of Nonferrous Metals Society of China, 2014, 24: 961−968.

[22] KEHOE S, ARDHAOUI M, STOKES J. Design of experiments study of hydroxyapatite synthesis for

orthopaedic application using fractional factorial design [J]. Journal of Materials Engineering and Performance, 2011, 20: 1423−1437.

[23] MATIN A, SANIEE F F, ABEDI H R. Microstructure and mechanical properties of Mg−SiC and AZ80-SiC nano-composites fabricated through stir casting method [J]. Materials Science and Engineering A, 2015, 625: 81−88.

[24] MOSES J J, DINAHARAN I, SEKHAR S J. Predicting the influence of process parameters on tensile strength of AA6061-TiC aluminum matrix composites produced using stir casting [J]. Transactions of Nonferrous Metal Society of China, 2016, 26: 1498−1511.

[25] THAHAMTAN S, HALVAEE A, EMAMY M, ZABIHI M S. Fabrication of Al/A206− Al_2O_3 nano/micro composite by combining ball milling and stir casting technology [J]. Materials and Design, 2013, 49: 347−359.

[26] SAJJADI S A, EZATPOUR H R, PARIZI M T. Comparison of microstructure and mechanical properties of A356 aluminum alloy/Al_2O_3 composites fabricated by stir and compo-casting processes [J]. Materials and Design, 2012, 34: 106−111.

[27] NAFISI S, EMADI D, SHEHATA M T, GHOMASHCHI R. Effects of electromagnetic stirring and superheat on the microstructural characteristics of Al−Si−Fe alloy [J]. Materials Science and Engineering A, 2006, 432: 71−83.

[28] SHU Shi-li, XING Bin, QIU Feng, JIN Shen-bao, JIANG Qi-chuan. Comparative study of the compression properties of TiAl matrix composites reinforced with nano-TiB_2 and nano-Ti_5Si_3 particles [J]. Materials Science and Engineering A, 2013, 560: 596−600.

[29] MAZAHERY A, ABDIZADEH H, BAHARVANDI H R. Development of high-performance A356/nano Al_2O_3 composites [J]. Materials Science and Engineering A, 2009, 518: 61−64.

[30] PUROHIT R, QURESHI M M U, DANDOUTIYA B K. Study of tribological properties of Al−Al_2O_3 nanocomposites developed through ultrasonic assisted stir casting process [J]. Materials Today: Proceedings, 2018, 5(9): 20492−20499.

[31] ABDIZADEH H, EBRAHIMIFARD R, BAGHCHESARA M A. Investigation of microstructure and mechanical properties of nano MgO reinforced Al composites manufactured by stir casting and powder metallurgy methods: A comparative study [J]. Composites: Part B, 2014, 56: 217−221.

[32] ZHONG X L, WONG W L E, GUPTA M. Enhancing strength and ductility of magnesium by integrating it with aluminum nanoparticles [J]. Acta Materialia, 2007, 55: 6338−6344.

[33] HALL E O. The deformation and ageing of mild steel: III discussion of results [J]. Proceedings of the Physical Society. Section B, 1951, 64: 747−753.

[34] PETCH N J. The cleavage strength of polycrystal [J]. Journal of Iron and Steel Research, International, 1953, 173: 25−28.

[35] ZHANG Z, CHEN D L. Contribution of Orowan strengthening effect in particulate-reinforced metal matrix nano composites [J]. Materials Science and Engineering A, 2008, 483−484: 148−152.

运用 D 实验设计优化电磁搅拌铸造 A357−SiC 纳米复合材料的力学性能

Reza MOHAMMADI BADIZI, Amir PARIZAD, Mohsen ASKARI-PAYKANI, Hamid Reza SHAHVERDI

Department of Materials Engineering, Tarbiat Modares University, P.O. Box 14115-143, Tehran, Iran

摘　要：采用 D 实验优化设计(DODOE)方法，对 A357−SiC 纳米复合材料的电磁搅拌铸造工艺进行研究。以 DX-7 软件获得的 9 个随机实验设计方案为主要目标，在 3 种不同的频率(10、35 和 60 Hz)下制备不同 SiC 含量(0.5%、1.0%和 1.5%，质量分数)的 A357−SiC 纳米复合材料。用扫描电镜和光学显微镜对其显微组织演变进行表征，并通过硬度和室温单轴拉伸试验对其力学性能进行研究。结果表明， SiC 纳米颗粒的均匀分布使材料的显微组织由枝晶向非枝晶态演化，晶粒尺寸减小 73.9%。此外，基于 DODOE 获得的屈服强度和极限抗拉强度的 *F* 值分别为 44.80 和 179.64，表明该模型具有显著性，变量(SiC 含量和搅拌频率)选取合适。结果表明，最佳搅拌频率为 60 Hz，最佳 SiC 含量为 1.5%(质量分数)，在此条件下，A357−SiC 纳米复合材料的屈服强度和极限抗拉强度分别为 120 和 188 MPa，比铸态试样的分别提高 57.7%和 57.9%。

关键词：A357 合金；电磁搅拌铸造；SiC 纳米颗粒；力学性能；D 实验优化设计

(Edited by Xiang-qun LI)